Total charge and mass changing cross sections of relativistic nuclei in hydrogen, helium, and carbon targets

W. R. Webber, J. C. Kish, and D. A. Schrier
Space Science Center, University of New Hampshire, Durham, New Hampshire 03824
(Received 19 December 1988)

This is the first in a series of papers describing the results of a systematic study of total, elemental, and isotopic cross sections measured in hydrogen, helium, and carbon targets. These fragmentation studies are based on measurements using 42 beams of 12 separate nuclei from ^{12}C to ^{58}Ni. This has resulted in the measurement of more than 100 secondary elemental cross sections and over 300 secondary isotopic cross sections in addition to the total charge changing and mass changing cross sections reported in this paper. These measurements have been made at energies from 300 to 1700 MeV/nucleon and include ten separate energies for ^{56}Fe, for example. The measurements have been made with the objective of interpreting the production of secondary nuclei during cosmic-ray propagation in the galaxy in order to better estimate the source elemental and isotopic composition of cosmic rays. At the same time they provide a valuable data base for nuclear physics and the understanding of peripheral interactions of energetic heavy nuclei. In the work reported in this paper ~ 100 total charge changing and mass changing cross sections have been measured for various targets and energies. The mass changing cross sections we measure are found to agree with earlier cross section measurements using energetic protons incident on targets composed of heavier elements to within $\sim 2\%$ in cases where a comparison can be made. The systematics of this new data set are described and a new, more accurate cross section formula is presented and discussed.

I. INTRODUCTION

Total inelastic charge changing and mass changing cross sections have been measured for incident ^{12}C, ^{14}N, ^{16}O, ^{20}Ne, ^{24}Mg, ^{27}Al, ^{28}Si, ^{32}S, ^{40}Ar, ^{40}Ca, ^{56}Fe, and ^{58}Ni nuclei with energies ranging from ~ 300 to 1700 MeV/nucleon in hydrogen (CH_2), helium, and carbon targets. These total cross sections were measured with an overall accuracy of $\sim 2\%$. This work is part of a systematic study of individual elemental and isotopic cross sections in hydrogen, helium, and carbon targets to be reported in several companion papers. These measurements are appropriate for interpreting the interstellar production of secondary nuclei during cosmic-ray propagation in the galaxy and so for determining the source elemental and isotopic composition of comic rays. At the same time it should be noted that the basic systematics of these cross sections as a function of incident charge, energy, and target are an important input for understanding theories of strong nuclear interactions. This data has been obtained over the course of 5 years of studies at the Lawrence Berkeley Laboratory Bevalac, with a total of 42 separate beams of various energies of the 12 charges listed earlier. The runs have all been made with a Cerenkov, scintillation counter telescope, directly in front of which are put the various targets of interest. These targets include CH_2, C, and He, generally ~ 0.5 of an interaction length thick. The choice of targets and their thickness, which is greater than customarily used, is optimized to obtain a high ratio of secondary production and to maximize the target in-target out ratio of events. This data will be compared with other total inelastic cross section measurements in similar targets and with models used to describe these cross sections as a function of incident charge, energy, and target.

II. THE EXPERIMENT AND MEASUREMENT TECHNIQUES

The configuration of detectors adopted for the cross section runs is shown in Fig. 1. The techniques for charge and mass measurement are similar to those used by our group to measure the charge and mass composition of primary cosmic rays in balloon borne telescopes.[1,2] The telescope basically consists of three separate modules. A charge identification module, an isotope identification module, and a fragment module. The Cerenkov x total energy technique[1] was used to identify the isotopes, and since it was necessary to stop the fragments in the total-energy counters, the arrangement of counters and absorbers differed slightly from run to run. For the study here only the charge detection module was used and this was unchanged except for the Cerenkov radiator for all of the runs. It consists of two CaF_2 scintillators, a Cerenkov counter, followed by a third CaF_2 scintillator. These counters have a resolution of $\lesssim 0.2$ charge unit for the scintillators and <0.1 charge unit for $\beta \rightarrow 1$ particles in the Cerenkov counter. Directly in front of this telescope were placed the different targets. The CH_2 and C targets were 7.5 cm diam disks of CH_2 and C of varying thickness. These target thicknesses were adjusted so that the energy loss in each type of target was the same. They were typically ~ 0.5 of an interaction length thick—necessary to provide enough in-

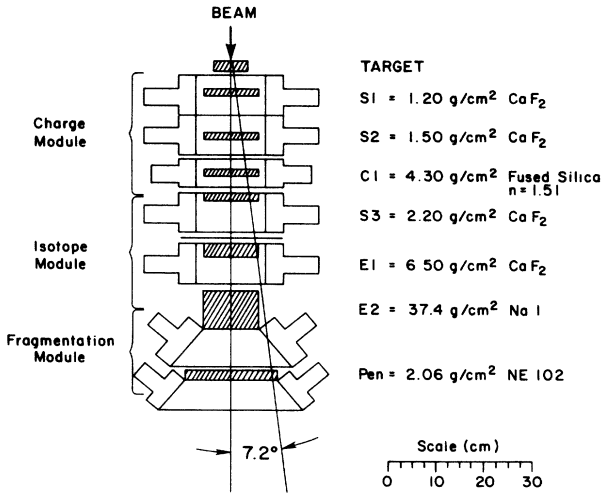

FIG. 1. Schematic drawing of the telescope.

teractions to measure the rarer isotopic cross sections. The hydrogen cross sections are obtained by a CH_2-C subtraction. A liquid-He target ~ 7 cm diam$\times 40$ cm long was also used and placed directly in front of the telescope. This target is described in more detail in Ferrando *et al.*[3]

Each beam was focused into a spot $\lesssim 2$ cm diam at the front of the target. For each beam energy the CH_2, C, and He targets were alternated with no target. Generally $\sim 3\times 10^5$ counts for each target run was obtained. The no target data is subtracted directly from the individual CH_2, C, and He target runs. The no target runs typically show $\lesssim 5\%$ interactions along the beam line and in the ~ 2.5 meters of air in front of the targets and in the $S1$ counter [see Figs. 2(a)–(c)].

The final element in the charge module defines an acceptance cone with a half-angle θ about the beam axis. For the He target this angle increases from 3.6° to 5.8° from one end of the target to the other. For the CH_2 and C targets $\theta \sim 7.7°$. These large acceptance angles insure that essentially all fragments considered in this work ($Z \geq 4$) are detected in the telescope. For all reactions this therefore becomes a measurement of the total cross section integrated over all angles. To be more specific, let us consider the worst case, i.e., $\theta = 3.6°$ and B nuclei at 600 MeV/nucleon. The maximum transverse momentum p_t, for B nuclei to be within the solid angle of the telescope and be detected is 470 MeV/c or ~ 2.7 times the 175 MeV/nucleon standard deviation of the typical measured Gaussian distribution,[4,5] indicating that less than 0.7% of the B fragments are out of the detector geometry. To test whether any interactions in the target were missing the telescope we placed, on several runs, a 2 in. diam scintillator in front of the target. All of the events recorded by this small counter were also observed in the telescope. These test runs were not used to determine cross sections.

Each counter in the telescope was coupled to a 4096 channel analyzer (12 bits) and a data word of approximately 200 bits was created for each event defined by a $S1-S3$ coincidence. The data system could handle ~ 1000 events per beam dump (every 5 sec). The average beam intensity was generally of this order so essentially full utilization of the beam was achieved. The data were stored event by event on magnetic tape and the data analysis was carried out by an IBM-PC computer.

III. DATA ANALYSIS AND DETERMINATION OF TOTAL FRAGMENTATION CROSS SECTIONS

Different analysis procedures are used to obtain the total interaction cross sections discussed in this paper and the charge and isotopic cross sections discussed in later papers.

A simple procedure is used to obtain the total interaction cross sections. In this case charge histograms are made directly from the $S1$ counter located next to the target. Examples of these histograms for C targets for incident beams of ^{16}O, ^{32}S, and ^{56}Fe nuclei are shown in Figs. 2(a)–(c). From this data the number of beam nuclei that survive passage through the target, N_z, can be determined from the total number of events in the beam charge peak, assuming a Gaussian shape for this peak. This number is compared with the total number of incident nuclei, N_B, as determined from the total number of events in the histograms. Histograms of the signals from $S1$ when no target is present [also shown in Figs. 2(a)–(c)] can then be used to correct for interactions along the beam line, in the 2.5 m of air before the target, and for interactions in $S1$. The measured numbers for each run are given in Table I for all beams and targets.

The total charge changing cross section, σ_z, of the beam nucleus in the target is readily obtained from the fraction f_z at the bottom of the target. In simple terms

$$\sigma_z = -\frac{m}{X_t}\ln f_z \ , \tag{1}$$

where m is the mass of the target nucleus and X_t is the target thickness in g/cm^2. In actual fact the calculation is somewhat more complicated because the no target data must be correctly accounted for. We write for the target runs

$$N_z^T = N_B^T \exp^{-X_t/\lambda_{zt}} \exp^{-X_{\rm tel}/\lambda_{\rm tel}} \ , \tag{2}$$

and for the no target run,

$$N_z^{\rm NT} = N_B^{\rm NT} \exp^{-X_{\rm tel}/\lambda_{\rm tel}} \ , \tag{3}$$

where $X_{\rm tel}$ is the thickness of $S1$+air and $\lambda_{\rm tel}$ is the interaction mean free path (MFP) in these materials and λ_{zt} is the MFP in the target. Taking the ratio of (2) and (3):

$$\frac{N_z^T}{N_z^{\rm NT}} = \frac{N_B^T}{N_B^{\rm NT}} \exp^{-X_T/\lambda_{zt}} \tag{4}$$

or

$$\lambda_{zt} = X_t / \ln\left[\frac{N_B^T}{N_z^T}\frac{N_z^{\rm NT}}{N_B^{\rm NT}}\right] \ , \tag{5}$$

where

$$\sigma_{zt}=\langle A^t\rangle/6.02\times10^{-4}\lambda_{zt}$$

and A^t is the average mass number of the target. In this way the cross section, σ_{zt}, is expressed in mb and λ_{zt} in g/cm^2. The cross sections measured in carbon and polyethylene (CH_2) allow us to deduce those in hydrogen from

$$\sigma_H=0.5(\sigma_{CH_2}-\sigma_C)\ . \tag{6}$$

The errors on all of the total cross sections are dominated by systematic errors, the largest of which are the no target corrections leading to an estimated uncertainty $\lesssim 1.2\%$, and the corrections of the beam charge distribution for events in the tail of the distribution, estimated to

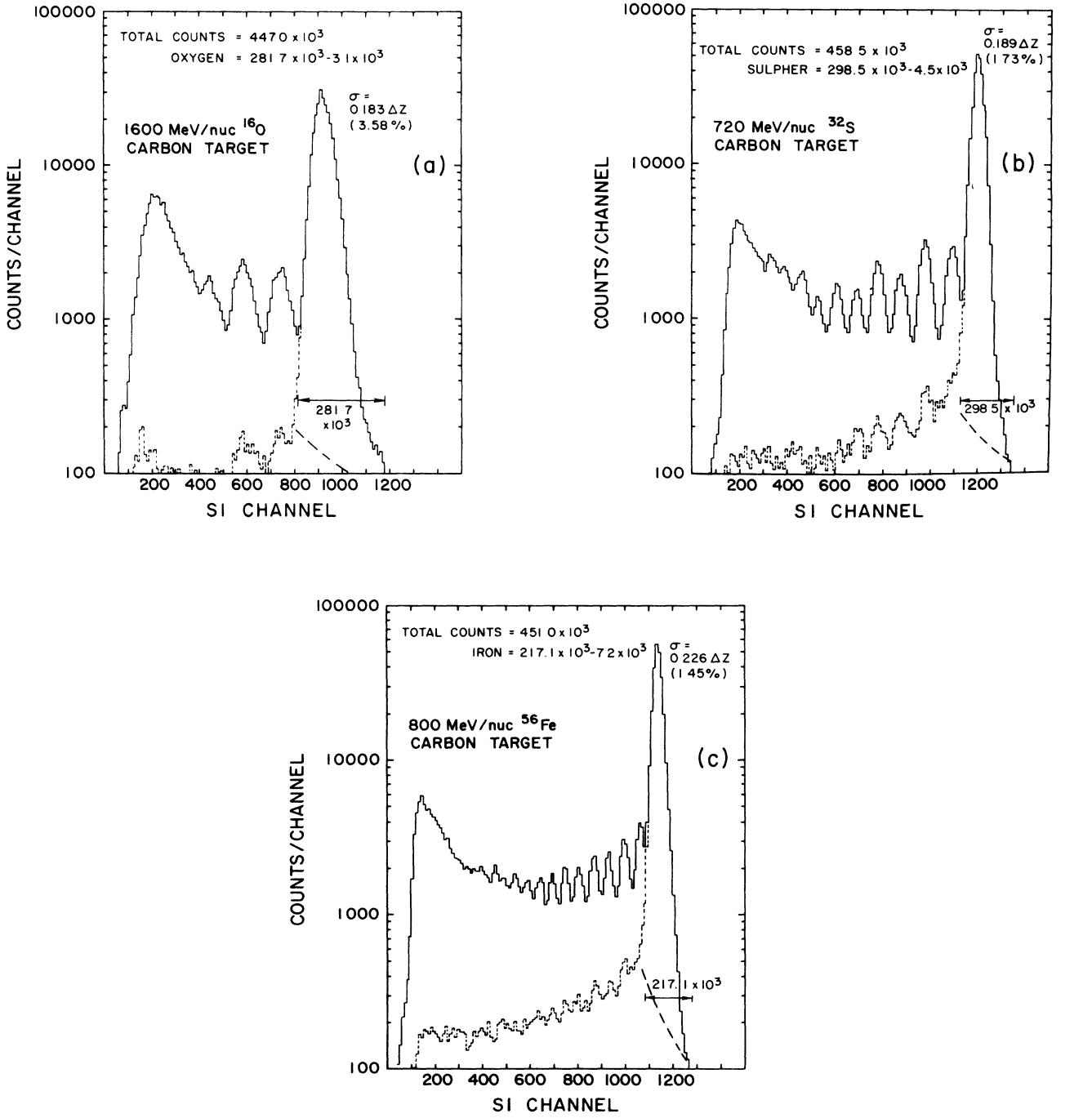

FIG. 2. (a) Charge histogram in $S1$ counter for ^{16}O fragmenting in carbon target along with no target data. (b) Charge histogram in $S1$ counter for ^{32}S fragmenting in carbon target along with no target data. (c) Charge histogram in $S1$ counter for ^{56}Fe fragmenting in carbon target along with no target data.

TABLE I. Measured quantities for various beams. Beam energy = energy incident upon target. Target energy = energy at midpoint of target.

Beam energy (MeV/nucleon)	Target energy (MeV/nucleon)	Poly Thickness (g/cm^2)	Poly N_z ($\times 1000$)	Poly N_B ($\times 1000$)	Poly N_B/N_z	Carbon Thickness (g/cm^2)	Carbon N_z ($\times 1000$)	Carbon N_B ($\times 1000$)	Carbon N_B/N_z
				Carbon beams					
450	296	8.75	36.0	52.2	1.4489	9.78	36.3	50.1	1.3813
435	326	8.75	150.0	217.5	1.4500	10.01	156.9	218.4	1.3917
435	403	6.01	365.3	477.4	1.3069	7.03	358.1	453.8	1.2673
450	418	6.01	226.0	295.3	1.3066	7.03	212.7	269.4	1.2665
610	561	11.08	264.2	434.9	1.6460	12.73	262.8	410.6	1.5624
730	693	8.75	136.2	208.6	1.5316	10.01	137.1	195.0	1.4222
950	915	8.75	216.4	331.9	1.5338	10.01	262.3	374.6	1.4280
1050	1016	8.75	261.3	402.9	1.5420	10.01	260.8	373.5	1.4323
1600	1572	8.75	279.1	435.3	1.5598	10.01	316.5	454.5	1.4361
				Nitrogen beam					
550	516	6.01	167.9	232.0	1.3815	7.03	181.8	241.0	1.3255
				Oxygen beams					
500	441	9.03	285.5	465.7	1.6313	10.73	299.0	458.4	1.5530
640	591	8.75	130.6	214.3	1.6409	10.01	137.3	207.5	1.5116
720	669	9.03	210.4	352.3	1.6747	10.73	183.2	284.5	1.5526
950	903	9.03	156.3	261.5	1.6734	10.73	87.2	135.0	1.5480
1600	1563	8.75	261.7	440.7	1.6833	10.01	278.6	427.4	1.5336
				Neon beams					
540	468	9.03	247.5	451.7	1.8252	10.73	106.3	176.9	1.6642
645	599	6.01	168.8	256.7	1.5206	7.03	161.4	228.0	1.4135
670	625	6.01	227.8	346.3	1.5199	7.03	196.6	277.5	1.4116
1096	1057	6.01	210.5	323.3	1.5358	7.03	216.5	307.5	1.4207
				Magnesium beams					
380	390	6.01	198.0	309.2	1.5618	7.03	209.3	308.0	1.4722
540	481	6.01	209.3	33.2	1.5921	7.03	341.5	508.4	1.4887
790	739	6.01	263.5	422.5	1.6034	7.03	316.6	469.7	1.4843
1500	1455	6.01	185.0	303.3	1.6403	7.03	187.5	279.4	1.4092
				Aluminum beam					
640	582	6.01	122.3	199.8	1.6339	7.03	191.0	286.9	1.5020
				Silicon beams					
570	503	6.01	334.3	550.7	1.6474	7.03	364.5	551.8	1.5138
830	770	6.01	280.7	465.1	1.6570	7.03	328.6	499.0	1.5183
1350	1296	6.01	129.2	218.4	1.6898	7.03	138.0	212.1	1.5363
				Sulfur beams					
720	649	6.01	277.0	486.9	1.7576	7.03	294.0	458.5	1.5595
1200	1138	6.01	213.3	376.5	1.7653	7.03	239.1	374.1	1.5646

TABLE I. (*Continued*).

Beam energy (MeV/nucleon)	Target energy (MeV/nucleon)	Poly Thickness (g/cm^2)	Poly N_z ($\times 1000$)	Poly N_B ($\times 1000$)	Poly N_B/N_z	Carbon Thickness (g/cm^2)	Carbon N_z ($\times 1000$)	Carbon N_B ($\times 1000$)	Carbon N_B/N_z
				Argon beams					
590	521	5.26	159.2	273.2	1.7158	6.15	161.1	243.2	1.5096
870	792	6.01	210.1	391.9	1.8659	7.03	191.4	311.2	1.6253
				Calcium beam					
760	672	6.01	193.6	362.1	1.8706	7.03	218.3	356.5	1.6330
				Iron beams					
400	330	2.51	136.0	184.9	1.3595	2.98	146.9	187.1	1.2737
540	439	4.84	167.2	306.8	1.8351	5.70	201.1	321.8	1.5986
580	518	2.75	293.6	419.6	1.4162	2.98	284.0	363.0	1.2783
600	521	3.51	367.6	574.6	1.5630	4.16	356.2	498.6	1.4008
810	724	6.01	209.9	451.0	2.1487	7.03	255.3	450.2	1.7635
1180	1086	6.01	188.5	405.3	2.1502	7.03	214.0	374.5	1.7507
1500	1409	6.01	153.7	335.3	2.1818	7.03	186.4	323.7	1.7650
1600	1512	6.01	237.2	517.0	2.1795	7.03	269.8	476.5	1.7661
1700	1615	6.01	87.4	191.2	2.1872	7.03	108.5	191.2	1.7620
				Nickel beam					
640	570	2.75	258.7	380.9	1.4722	3.26	284.2	380.0	1.3372

produce an uncertainty $\lesssim 1.5\%$ (see Figs. 2(a)–(c). The quoted errors include these uncertainties added in quadrature with 2 times the statistical error on the number of events (see Table I) or the difference in the number of events in the case of hydrogen. The charge changing cross sections and MFP for CH_2, C, H, and He targets derived from the data in Table I are listed in Table II. In Table III we separately list the cross sections obtained for hydrogen targets and the ratios of σ_{He} and σ_C to σ_H. The values for σ_{He} and the parameters associated with these measurements have also been given in a separate paper by Ferrando *et al.*[3] Finally in Table IV we show the charge changing cross sections adjusted to a common energy of 1500 MeV/nucleon, where the cross sections are approaching their asymptotic high-energy limit. These cross sections are derived by fitting smooth curves to the energy dependent cross sections as discussed in the next section.

We should remark that these cross sections are defined to be the cross sections for the removal of at least one charge from the projectile, $\sigma_{\Delta Z \geq 1}$. This is the cross section that is usually measured and quoted in the literature when incident beams of heavy nuclei have been used, e.g., Westfall *et al.*[6] Another relevant quantity is the mass changing cross section, $\sigma_{\Delta A \geq 1}$, which is defined as the cross section for removing at least one nucleon. In trying to parametrize these cross sections, and for understanding their systematics as well as for propagation studies it is important to distinguish between these two types of cross sections. We also believe that the mass changing cross sections most closely correspond to the extensive data on total inelastic cross sections derived when protons of various energies are incident on heavier targets.

Our experiment permits the identification of the isotopes of the beam charge that have fragmented. This analysis is described in a later paper of this series. However, we believe it is important to describe and discuss the total mass changing cross sections here as well. These cross sections have been determined systematically at one energy, ~600 MeV/nucleon, where the neutron stripping cross sections have been measured. We show in Table V these total mass changing cross sections including the addition due to the neutron stripping cross sections. Also shown are the new ratios σ_{He}/σ_H and σ_C/σ_H for these mass changing cross sections.

IV. SYSTEMATICS OF THE CROSS SECTIONS AND A COMPARISON WITH OTHER CROSS SECTION MEASUREMENTS

A. Charge changing cross sections

The cross-section data set on total charge changing and mass changing cross sections we have assembled is perhaps the most comprehensive available for heavier nuclei incident on H, He, and C targets in terms of the number of different incident nuclei and the different energies involved. Other comparable studies we should mention include cross sections derived from 1.88 GeV/nucleon ^{56}Fe nuclei incident on ten different targets (Westfall *et al.*[6]) and a study of Kr, Xe, Ho, and Au nuclei frag-

TABLE II. Measured values of λ and σ for various beams. (Errors: $A = \pm 0.7-1.0\,\%$, $B = \pm 1.0-1.5\,\%$, and $C = \pm 1.5-2.5\,\%$).

Target energy (MeV/nucleon)	Poly target λ (g/cm)	Poly target σ (mb) (error)	Carbon target λ (g/cm)	Carbon target σ (mb) (error)	H target σ (mb) (error)	Helium target λ (g/cm)	Helium target σ (mb) (error)
			Carbon beams				
296	23.86 (*A*)	974 (*A*)	30.27 (*A*)	658 (*A*)	158 (*C*)		
326	23.55 (*A*)	988 (*A*)	30.31 (*A*)	658 (*A*)	165 (*C*)		
403	22.45 (*A*)	1036 (*A*)	29.67 (*A*)	672 (*A*)	181 (*C*)		
418	22.53 (*A*)	1035 (*A*)	29.76 (*A*)	670 (*A*)	183 (*C*)		
561	20.67 (*A*)	1125 (*A*)	28.53 (*A*)	699 (*A*)	213 (*C*)	17.02 (*B*)	397 (*B*)
693	20.52 (*A*)	1133 (*A*)	28.42 (*A*)	703 (*A*)	215 (*C*)		
915	20.46 (*A*)	1137 (*A*)	28.13 (*A*)	709 (*A*)	212 (*C*)	15.72 (*B*)	421 (*B*)
1016	20.20 (*A*)	1151 (*A*)	27.86 (*A*)	716 (*A*)	218 (*C*)		
1572	19.68 (*A*)	1182 (*A*)	27.68 (*A*)	721 (*A*)	231 (*C*)	15.28 (*B*)	433 (*B*)
			Nitrogen beam				
516	18.60 (*A*)	1251 (*A*)	24.95 (*A*)	796 (*A*)	227 (*C*)	13.97 (*B*)	475 (*B*)
			Oxygen beams				
441	18.45 (*A*)	1260 (*A*)	25.11 (*A*)	794 (*A*)	232 (*C*)		
591	17.87 (*A*)	1316 (*A*)	24.24 (*A*)	823 (*A*)	247 (*C*)	12.96 (*B*)	509 (*B*)
669	17.51 (*A*)	1328 (*A*)	24.39 (*A*)	817 (*A*)	253 (*C*)		
903	17.54 (*A*)	1326 (*A*)	24.56 (*A*)	813 (*A*)	248 (*C*)		
1563	16.79 (*A*)	1385 (*A*)	23.44 (*A*)	851 (*A*)	269 (*C*)	13.03 (*B*)	522 (*B*)
			Neon beams				
468	15.01 (*A*)	1550 (*A*)	20.98 (*A*)	951 (*A*)	298 (*C*)		
599	14.34 (*A*)	1619 (*A*)	20.32 (*A*)	980 (*A*)	319 (*C*)		
625	14.35 (*A*)	1621 (*A*)	20.38 (*A*)	977 (*A*)	378 (*C*)		
1057	14.00 (*A*)	1662 (*A*)	19.98 (*A*)	998 (*A*)	330 (*C*)		
			Magnesium beams				
309	13.49 (*A*)	1725 (*A*)	18.18 (*A*)	1097 (*A*)	310 (*C*)		
481	12.92 (*A*)	1800 (*A*)	17.67 (*A*)	1128 (*A*)	336 (*C*)		
739	12.73 (*A*)	1826 (*A*)	17.92 (*A*)	1120 (*A*)	358 (*C*)		
1455	12.12 (*A*)	1915 (*A*)	17.86 (*A*)	1133 (*A*)	391 (*C*)		
			Aluminum beam				
582	12.24 (*A*)	1899 (*A*)	17.28 (*A*)	1154 (*A*)	373 (*C*)	8.67 (*B*)	766 (*B*)
			Silicon beams				
503	12.04 (*A*)	1933 (*A*)	16.95 (*A*)	1176 (*A*)	379 (*C*)		
770	11.89 (*A*)	1956 (*A*)	16.83 (*A*)	1183 (*A*)	387 (*C*)		
1296	11.47 (*A*)	2027 (*A*)	16.41 (*A*)	1215 (*A*)	407 (*C*)		
			Sulfur beams				
649	10.66 (*A*)	2181 (*A*)	15.82 (*A*)	1260 (*A*)	460 (*C*)		
1138	10.57 (*A*)	2200 (*A*)	15.71 (*A*)	1269 (*A*)	466 (*C*)		
			Argon beams				
521	9.74 (*A*)	2387 (*A*)	14.69 (*A*)	1357 (*A*)	514 (*C*)		
792	9.64 (*A*)	2414 (*A*)	14.46 (*A*)	1378 (*A*)	518 (*C*)		
			Calcium beam				
672	9.60 (*A*)	2423 (*A*)	14.34 (*A*)	1390 (*A*)	517 (*C*)		
			Iron beams				
330	8.17 (*B*)	2846 (*B*)	12.21 (*B*)	1632 (*B*)	608 (*C*)		
439	7.97 (*A*)	2917 (*A*)	12.05 (*A*)	1654 (*A*)	632 (*C*)	6.04 (*B*)	1100 (*B*)
518	7.91 (*A*)	2939 (*A*)	12.15 (*A*)	1640 (*A*)	650 (*C*)		
521	7.86 (*A*)	2958 (*A*)	12.01 (*A*)	1663 (*A*)	648 (*C*)		
724	7.86 (*A*)	2958 (*A*)	12.40 (*A*)	1607 (*A*)	676 (*C*)	5.90 (*B*)	1126 (*B*)
1086	7.85 (*B*)	2962 (*B*)	12.56 (*B*)	1587 (*B*)	687 (*C*)		
1409	7.70 (*A*)	3019 (*A*)	12.37 (*A*)	1611 (*A*)	704 (*C*)		
1512	7.71 (*A*)	3016 (*A*)	12.33 (*A*)	1616 (*A*)	700 (*C*)		
1615	7.68 (*A*)	3027 (*A*)	12.46 (*A*)	1598 (*A*)	714 (*C*)	5.54 (*B*)	1199 (*B*)
			Nickel beam				
570	7.11 (*B*)	3271 (*B*)	11.22 (*B*)	1777 (*B*)	767 (*C*)		

TABLE III. Ratios of helium and carbon cross sections to hydrogen cross section. [Errors: $A = \pm(2.0-3.0)\%$, and $B = \pm(2.5-3.5)\%$.]

Target energy (MeV/nucleon)	Hydrogen σ (mb)	He/H cross section ratio (error)	C/H cross section ratio (error)
	Carbon beams		
296	158		4.16 (*A*)
326	165		3.97 (*A*)
403	181		3.72 (*A*)
418	183		3.66 (*A*)
561	213	1.85 (*B*)	3.30 (*A*)
693	215		3.27 (*A*)
915	212	1.97 (*B*)	3.33 (*A*)
1016	218		3.28 (*A*)
1572	231	1.87 (*B*)	3.12 (*A*)
	Nitrogen beam		
516	227	2.07 (*B*)	3.42 (*A*)
	Oxygen beams		
441	232		3.42 (*A*)
591	247	2.05 (*B*)	3.33 (*A*)
669	253		3.23 (*A*)
903	249		3.26 (*A*)
1563	269	1.95 (*B*)	3.16 (*A*)
	Neon beams		
468	298		3.19 (*A*)
599	318		3.08 (*A*)
625	318		3.05 (*A*)
1057	330		2.99 (*A*)
	Magnesium beams		
309	330		3.53 (*A*)
481	336		3.36 (*A*)
739	358		3.13 (*A*)
1455	383		2.91 (*A*)
	Aluminum beam		
582	373	2.04 (*B*)	3.09 (*A*)
	Silicon beams		
503	379		3.10 (*A*)
770	387		3.06 (*A*)
1296	408		2.95 (*A*)
	Sulfur beams		
649	460		2.74 (*A*)
1138	466		2.73 (*A*)
	Argon beams		
521	514		2.64 (*A*)
792	518		2.66 (*A*)
	Calcium beam		
672	516		2.69 (*A*)
	Iron beams		
330	608		2.68 (*B*)
439	632	1.74 (*B*)	2.62 (*A*)
518	650		2.52 (*A*)
521	648		2.57 (*A*)
724	676	1.67 (*B*)	2.38 (*A*)
1086	687		2.31 (*A*)
1409	704		2.29 (*A*)
1512	700		2.31 (*A*)
1615	714	1.68 (*B*)	2.24 (*A*)
	Nickel beam		
570	767		2.31 (*B*)

mentation at ~1 GeV/nucleon for Al, C, and CH_2 targets (Binns *et al.*[7]). A large number of cross sections have also been measured using energetic protons incident on a large number of targets. For example, at energies between 220–570 MeV/nucleons by Renberg *et al.*,[8] and at high energies, $\gtrsim 4$ GeV/nucleon, by Bobchenko *et al.*[9] Previous cross-section measurements for hydrogen targets (using mainly energetic proton beams) have been summarized and a semiempirical proton-nucleus cross-section formula presented by Letaw *et al.*[10] These authors also note that there is a scarcity of data in the region from ~500 MeV to a few GeV/nucleon, a region well covered by our new data.

Our data for total charge changing cross sections is summarized for carbon targets as a function of incident energy for the 12 separate beams in Fig. 3. The hydrogen cross sections are shown in Fig. 4. If other total charge changing cross section measurements for carbon and hydrogen targets obtained using energetic heavy-ion beams—e.g., Westfall *et al.*,[6] or Brechtmann and Heinrich,[11] are compared with our data, the agreement is good within the limited accuracy of the other data which is ~5–10%.

A comparison of our data with hydrogen cross sections measured using energetic proton beams incident on various targets is somewhat more difficult because, for one thing, it is not always clear whether the experimenters using proton beam actually obtained mass changing or charge changing cross sections or whether the cross sections they obtained are precisely equivalent to those we derive. The high-energy cross sections for hydrogen obtained from a condensation of the data from Bobchenko *et al.*,[9] are shown in Table IV along with our derived charge changing cross sections 1.5 GeV/nucleon. It is seen that the Bobchenko *et al.* values are, on average, 9±2% higher than those we obtain. Part, or all, of this difference could be due to the fact that the cross sections are still increasing toward an asymptotic high-energy value above ~1.5 GeV/nucleon. Or it could be due to a different definition of the total cross section as noted before. In this connection it should also be noted that the hydrogen cross sections obtained by Renberg *et al.*,[8] between ~200 and 600 MeV/nucleon for C, O, Al, and Fe targets also average ~9±2% higher than the charge changing cross sections we measure as shown in Figs. 3 and 4. A comparison of these measurements and our values for some charge changing cross sections for H targets is shown in Fig. 5. We will return to this comparison later when we discuss the mass changing cross sections, but meanwhile we discuss in more detail the systematics of our total charge changing cross section measurements.

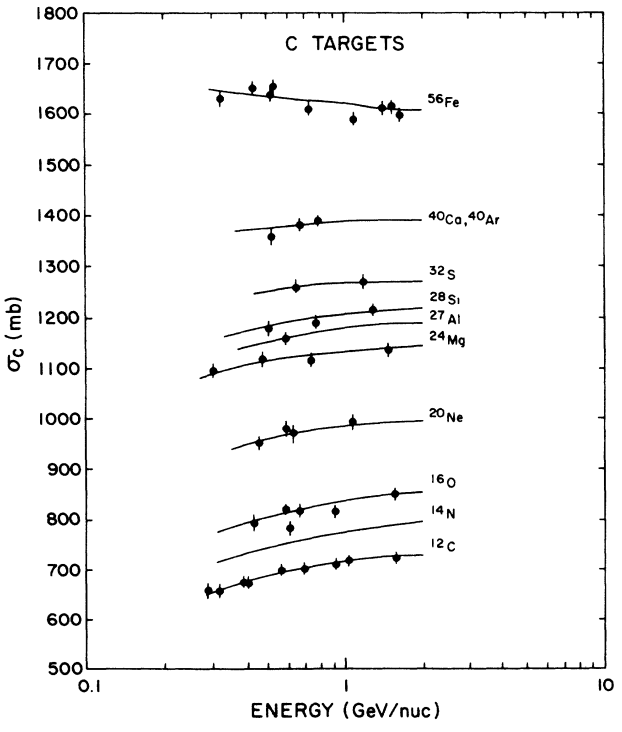

FIG. 3. Charge changing cross sections in carbon targets for various beams and energies.

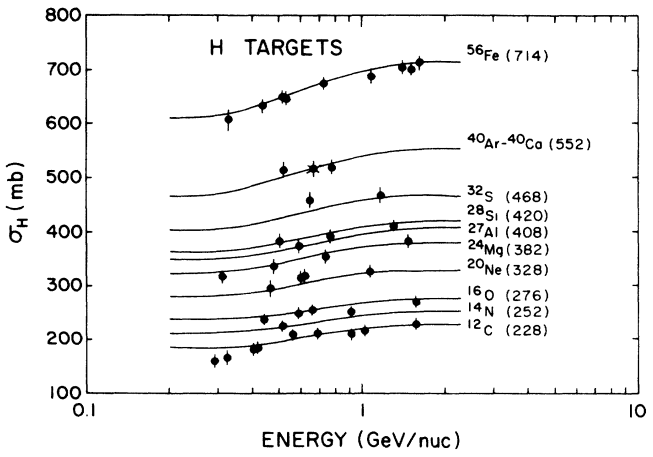

FIG. 4. Charge changing cross sections in hydrogen targets for various beams and energies. Numbers in parenthesis refer to best-fit cross sections in mb at 1500 MeV/nucleon.

Consider first the energy dependence of the cross sections. A very distinct energy dependence is observed for all incident beam charges in hydrogen targets in the energy range 300–1600 MeV/nucleon as seen in Fig. 4. The data is in excellent agreement with the solid lines in Fig. 4 that represent the parametrized fits to all of the available data below ~2 GeV/nucleon as derived by Letaw *et al.*[10] As noted earlier, this energy dependent parametrization is based entirely on data obtained using energetic proton beams incident on heavier targets, which leads to cross sections ~9% larger than the charge changing cross sections we measure, so we have multiplied the Letaw *et al.* cross sections by 0.91 to fit with our measured charge changing cross section data.

Turning now to the energy dependence of the cross sections obtained in carbon targets as shown in Fig. 3, we notice a somewhat different energy dependence. For lower Z incident beams an energy dependence similar to that for hydrogen targets is observed, however for in-

TABLE IV. Charge changing cross sections at 1500 MeV/nucleon (in mb).

Charge	σ_H	σ_H[a]	σ_{He}	σ_C	σ_C/σ_H
^{12}C	228±4	251±2	431±7	725±9	3.18
^{14}N	252±4		482±8	796±10	3.16
^{16}O	275±5		512±9	850±10	3.09
^{20}Ne	328±6			992±12	3.02
^{24}Mg	382±7	422±5		1140±14	2.98
^{27}Al	406±7	456±6	796±12	1188±16	2.93
^{28}Si	418±7			1216±16	2.91
^{32}S	469±8	514±6		1270±17	2.71
^{40}Ar	548±9			1390±19	2.54
^{40}Ca	548±9	603±6		1390±19	2.54
^{56}Fe	714±11	760±8	1196±21	1615±20	2.26
^{58}Ni	783±15			1745±25	2.20

[a]Bobchenko *et al.* (Ref. 9).

cident Fe the total charge changing cross sections are almost independent of energy, perhaps even rising slightly at the lowest energies. This has important implications with regard to the propagation of cosmic-ray nuclei through air, for example. It already shows that simple scaling factors for obtaining the cross sections in air from those in hydrogen or vice versa are inadequate. This is further borne out by Fig. 6, which shows the ratio of the measured carbon cross sections to those in hydrogen, and also the helium to hydrogen cross sections as a function of energy. There is an obvious systematic behavior of these ratios that is a function of energy, incident charge, and target. From a study of Fe fragmentation at one energy, 1.88 GeV/nucleon, in a variety of targets, Westfall *et al.*,[6] have suggested that the individual elemental charge changing cross sections could be factored into a target factor γ_T, depending upon the target only, and a factor γ_B^i, which depends on the beam and fragment, e.g., $\sigma_{BT}^i = \gamma_T \cdot \gamma_B^i$. Such a factorization is expected at high energies from a variety of theoretical arguments and, if applicable, greatly simplifies the scaling of cross sections to other targets or beams. The application of this factorization to individual elemental cross sections at lower energies will be considered in paper II; here we consider its relationship and applicability to the total cross sections. In simple terms, factorization means that the ratio of the individual elemental cross sections, σ_{BT}^i to the total cross sections σ_{BT} may be expressed as a fraction that is independent of energy. It is evident from the strong dependence on energy of the σ_C/σ_H and σ_{He}/σ_H ratios illustrated in Fig. 6, particularly for lower Z incident particles, that a simple factorization cannot apply to the total charge changing cross sections over the entire energy range, although it could certainly apply at high energies, where the ratios are nearly constant. For example, our value of 2.26±0.06 for the σ_C/σ_H cross section ratio at high energies for a ^{56}Fe beam compares well with the ratio of 2.29±0.15 measured by Westfall *et al.*[6] Note, however, that the target factor for fragments with $Z = 18-24$ obtained by Westfall *et al.*,[6] is 1.92±0.09.

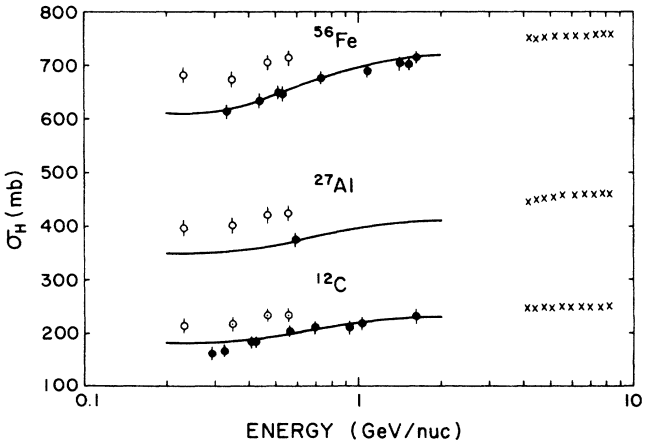

FIG. 5. Charge changing cross sections in hydrogen targets for selected beams and energies. Data from Renberg *et al.* (Ref. 8) (ϕ) and Bobchenko *et al.* (Ref. 9) ($\times\times\times$) using energetic proton beams are also shown for various targets corresponding to the charges we measure.

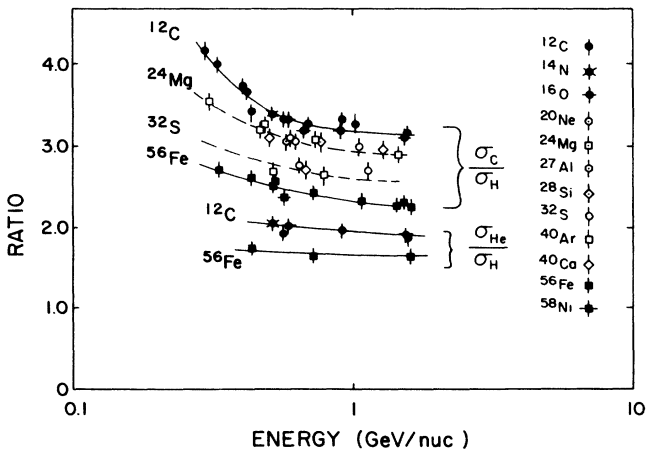

FIG. 6. Ratios of total charge changing cross sections in C and H and in He and H targets as a function of energy.

Thus in order to achieve the observed total cross section ratio of 2.26, this target factor must increase for lower Z fragments even for their analysis.

Our value of 1.65 ± 0.08 for the σ_{He}/σ_{H} cross section ratio was not directly measured by Westfall *et al.*, but an interpolated value of this ratio from their data is 1.62.

Westfall *et al.*[6] suggest that the target factor γ_T scales with target mass number A_T in a manner similar to that commonly used for the total cross sections, e.g., $\gamma_T = a A_T^d$, or by a linear relationship

$$\gamma_T = C(A_T^{1/3} + A_B^{1/3} - b) ,$$

similar to the overlap equation

$$\sigma_{BT} = C(A_t^{1/3} + A_B^{1/3} - b)^2 \quad (7)$$

commonly used to calculate the total cross sections. Our measurements with many beams of C, He, and H targets allow us to examine this dependence in unprecedented detail and accuracy. In Fig. 7 we show our measured total charge changing cross sections extrapolated to a common energy of 1500 MeV/nucleon for the C, He, and H targets for all the 12 incident beams. For H and He targets this data as a function of A_B is well fit by straight lines with slopes of 0.75 ± 0.02 and 0.66 ± 0.02, respectively. For a carbon target the best-fit straight line has a slope of 0.55 ± 0.02, but a slightly curved line would be a better fit to the data. Note, particularly, that these fits do not all have the same slope, an observation that would be expected from the cross section ratios presented in Table IV or Fig. 6. In Fig. 7 we have also included other comparable cross section data for higher A_B. Of particular interest here are the measurements using higher Z beams by Binns *et al.*[7] It is evident here that, although the description of these cross sections by a constant exponent dependence on A_B is generally a good approximation for $A_B \leq 60$, it cannot hold over the entire range of A_B. One needs to consider expressions with a mass dependent overlap parameter to produce a fit to this data and also to the data for carbon targets for lower Z incident beams (e.g., Binss *et al.*[7]).

B. Mass changing cross sections

We now turn our attention to the total mass changing cross sections, which as we have noted earlier, may correspond more closely to the total inelastic cross sections obtained using energetic proton beams incident on various targets. As part of the measurement of the individual elemental and isotopic cross sections we have determined the neutron stripping cross sections for the various beam nuclei—mainly at energies ~600 MeV/nucleon. This work is described in more detail in another paper of this series,[12] here we show in Table V the total mass changing cross sections at 600 MeV/nucleon for H, He, and C targets (and in parenthesis for each case we show the sum of all neutron stripping cross sections). These total mass changing cross sections are plotted as a function of A_B in Fig. 8. Again this data is well fit by straight lines corresponding to a form $\sigma_{ABT} = a A_B^d$. The best fits to the data at 600 MeV/nucleon obtained using this expression are shown in Table VI, where the best fits to the data on charge changing cross sections at 1500 MeV/nucleon are also shown. To directly compare these two sets of cross sections at a common energy we need to consider the en-

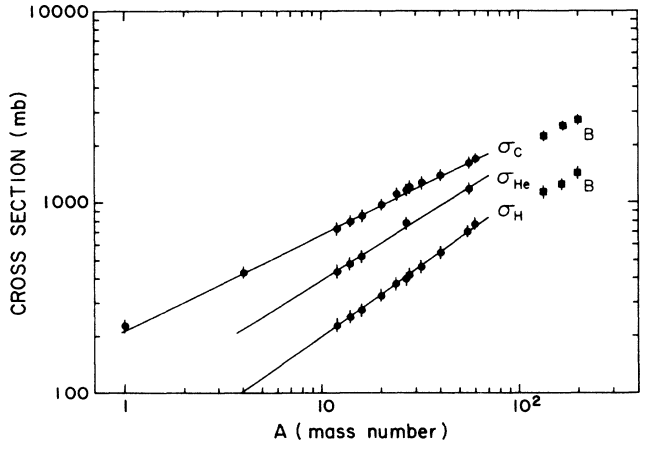

FIG. 7. Charge changing cross sections at 1500 MeV/nucleon for beams with $A = 4 - \sim 200$ for H, He, and C targets. Data for high Z beam nuclei from Binns *et al.* (Ref. 7), B is also shown.

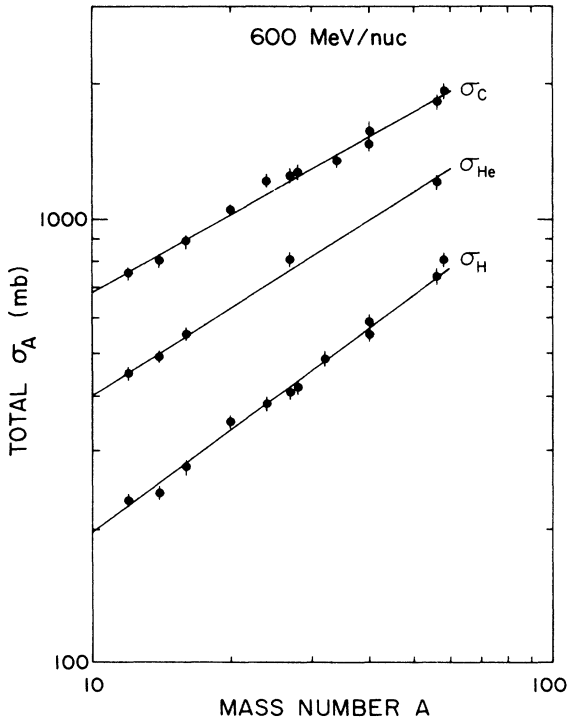

FIG. 8. Mass changing cross sections at 600 MeV/nucleon as a function of incident beam as measured in this experiment for H, He, and C targets.

TABLE V. Total mass changing σ in mb at ~600 MeV/nucleon. [(+) represents the sum of all neutron stripping cross sections.]

	σ_{AH}	σ_{AHe}	σ_{AHe}/σ_{AH}	σ_{AC}	σ_{AC}/σ_{AH}
^{12}C	242.5(+28.2)	453(+46.5)	1.88	757(+61.5)	3.13
^{14}N	242(+8.6)	468(+10.9)	2.05	802(+15.2)	3.36
^{16}O	275.5(+27.5)	554(+45.3)	2.03	891(+74.2)	3.27
^{20}Ne	348(+31.8)			1056(+78.3)	3.05
^{24}Mg	381(+34.7)			1218(+90.3)	3.19
^{27}Al	408(+34.9)	805(+39.6)	1.97	1232(+75.6)	3.03
^{28}Si	415(+32.5)			1271(+91.1)	3.05
^{32}S	492(+34.9)			1338(+78.9)	2.72
^{40}Ar	596(+93.0)			1595(+231.1)	2.68
^{40}Ca	542(+23.5)			1457(+66.6)	2.69
^{56}Fe	736(+75.3)	1136(+106.2)	1.53	1826(+196.3)	2.48
^{58}Ni	812(+65.0)			1949(+192.5)	2.40

ergy dependence of the mass charging cross sections. We have our own measurements of the energy dependence of the charge changing cross sections, which we noted earlier were consistent with the energy dependence used by Letaw *et al.*,[10] to describe the total inelastic cross sections in hydrogen. If we use the factor 1.092, obtained by Letaw *et al.*[10] for hydrogen targets, then the expression for the total mass changing cross section at 1500 MeV/nucleon we derive from our data is $\sigma_A = 40.7 A_B^{0.73}$ mb. By taking this energy dependence factor to be the same as measured by charge changing cross sections, one is assuming that the neutron stripping cross section is a constant fraction of the total charge changing cross section at all energies. Data on this neutron stripping cross section as a function of energy is very limited, but comparing our measurements at 600 MeV/nucleon with those of Lindstrom *et al.*,[13] at 2.1 GeV/nucleon, for ^{16}O and ^{12}C beams incident on hydrogen targets, shows that this is a very good approximation. In any case, the total neutron stripping cross section are ~10% of the total charge changing cross sections, so that a small error here will not have a large effect on the 1500 MeV/nucleon mass changing cross sections we derive.

In Table VII we compare the 1500 MeV/nucleon total mass changing cross sections we derive for hydrogen targets with the most comprehensive ones available, those of Bobchenko *et al.*,[9] and with the empirical formula obtained by Letaw *et al.*,[10] which is claimed to have an average accuracy ~1.5%. It is seen that our formula provides a slightly better overall fit to the Bobchenko *et al.* data for $A_B \lesssim 60$ than does the formula of Letaw *et al.*[10] It also confirms our earlier suggestion that the total mass changing cross sections derived from heavy-ion beams incident on hydrogen targets are most directly comparable to the total inelastic cross sections derived from energetic proton beams incident on heavy targets—in this case the two sets of cross sections are consistent to within an average ~1%. To derive a corresponding energy correction factor between 600 and 1500 MeV/nucleon for the mass changing cross sections in He and C targets we make use of the data shown in Fig. 6 on the σ_{He}/σ_H and σ_C/σ_H ratios. We again assume that the energy dependent factor we measure for charge changing cross sections is the same for mass changing cross sections. The energy dependence of the ratios observed in Fig. 6 implies that the energy factor between 600 and 1500 MeV/nucleon for He and C targets is less than for hydrogen targets. The ratio we derive for He targets is 1.040 and for carbon targets 1.026 (cf. Table VI). It is sensibly independent of beam charge above ~600 MeV/nucleon. Note that the A_B dependence of the σ_{He}/σ_H and σ_C/σ_H ratios observable in the data in Fig. 6 is a direct measure of the different exponents in the A_B dependence of the cross sections for the different targets.

V. PARAMETRIZATION OF THE TOTAL CROSS SECTIONS

The parametrization of the total cross sections is of fundamental importance in the propagation of energetic particles through matter, including the estimation of ra-

TABLE VI. Dependence of σ on A_B.

	Charge changing σ	Mass changing σ		
Target	1500 MeV/nucleon	600 MeV/nucleon	Factor 1500	MeV/nucleon
Hydrogen	$34.9 A_B^{0.75}$	$37.3 A_B^{0.73}$	1.092[a]	$40.7 A_B^{0.73}$
Helium	$88.7 A_B^{0.64}$	$93.1 A_B^{0.64}$	1.040	$96.8 A_B^{0.64}$
Carbon	$188.1 A_B^{0.55}$	$184.8 A_B^{0.57}$	1.026	$189.6 A_B^{0.57}$

[a]From Letaw *et al.* (Ref. 10).

TABLE VII. Total mass changing σ for hydrogen targets at 1500 MeV/nucleon (in mb).

	$40.7A^{0.73}$ this work	Bobchenko *et al.* (Ref. 9)	$44.9A^{0.70}$ Letaw *et al.* (Ref. 10)
^{12}C	250	251±2	256
^{14}N	279		285
^{16}O	308		313
^{20}Ne	363		366
^{24}Mg	414	422±5	415
^{27}Al	451	456±7	451
^{28}Si	464		463
^{32}S	511	514±6	508
^{40}Ar	601		601
^{40}Ca	601	603±6	594
^{56}Fe	769	760±8	752
^{58}Ni	789		770
^{63}Cu	(838)	831±8	817

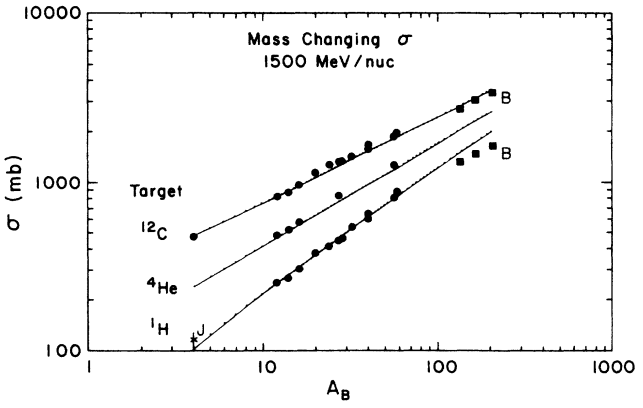

FIG. 9. Mass changing cross sections at 1500 MeV/nucleon for incident beams with $A=4-\sim 200$ for H, He, and C targets. Symbols the same as in Fig. 7. Predictions of cross sections using Eq. (10) shown as a solid line.

diation effects in materials. It is also of importance in deriving theoretical models to explain the nuclear interaction process (e.g., Karol[14]). The earliest attempts, valid generally at high energies, were of the form

$$\sigma_{BT}=C(A_T^{1/3}+A_B^{1/3}-b)^2 \text{ mb} . \quad (8)$$

This formula recognizes the fact that the classical radius of a nucleus is $\sim A^{1/3}$ and also that in a nuclear interaction there is a transparency factor or overlap factor, designated here by b, which reduces the cross section. This formula effectively predicts the total cross sections for a given target will be $\sim A_B^{0.67+\delta}$, where δ depends on the overlap parameter. The most comprehensive attempt to parametrize the cross sections for hydrogen targets as a function of both energy and A_B was by Letaw *et al.*[10] who derived a best fit with $\sigma\sim A_B^{0.70}$ at high energies along with an energy dependent factor. Recently, Binns *et al.*,[7] measured the charge changing cross sections in several targets using very heavy ions with $Z=36-79$. They found, as our data also shows, that both a target and beam dependent overlap parameter is required to fit the data, and used a relation of the form

$$\sigma_{BT}=C[A_T^{1/3}+A_B^{1/3}-p(A_T+A_B)^q]^2 \text{ mb} . \quad (9)$$

They found that, if $q=\frac{1}{3}$ then $p=0.209$, although in practice these constants are not completely independent. This expression does not extrapolate well to our mass region and particularly to the effects we observe independently as a function of both A_B and A_T. Physically this suggests an overlap model with the overlap dependent separately on the masses of both nuclei involved:

$$\sigma_{BT}=C\{A_T^{1/3}+A_B^{1/3} -[(t_0-tA_t)-(b'A_B^{1/3}A_t^{1/3})]\}^2 \text{ mb} . \quad (10)$$

This could also be written as an expression of the form

$$\sigma_{BT}=a(A)A_B^{2/3\delta(A_B+A_T)}$$

to simply fit the data as was done in Table VII, but we believe that the overlap expression has a more physical interpretation.

In order to facilitate comparison with the data, we show the total mass changing cross sections at 1500 MeV/nucleon in Fig. 9. These are essentially the mass changing cross sections at 600 MeV/nucleon shown in Fig. 8, with the correction factor to high energies as described earlier in conjunction with Table VII. For the total charge changing cross sections for high Z nuclei presented by Binns *et al.*,[7] we have obtained total mass changing cross sections equivalent to ours by assuming (1) the neutron stripping cross sections are the same fraction of the total charge changing cross sections as we measure for ^{56}Fe; (2) the correction factor to 1500 MeV/nucleon for their data is the same as we obtain for lower Z nuclei in hydrogen, helium, and carbon targets.

In Fig. 9, we also show the predicted cross sections using Eq. (10) with $t_0=1.36$, $t=0.018$, and $b'=0.065$ ($C=57.3$ corresponding to a nuclear radius of 1.35 fm).

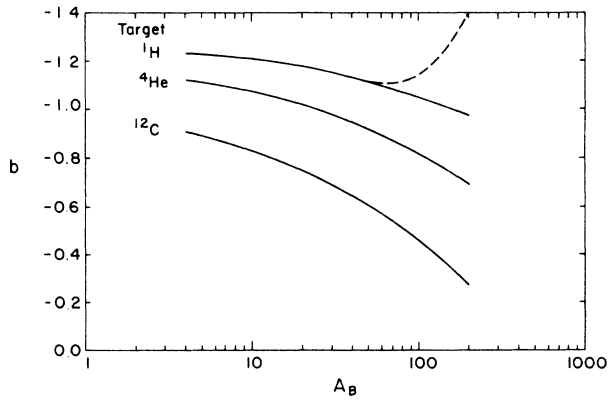

FIG. 10. The value of b, the overlap parameter, calculated using Eq. (10), as a function of A_B for H, He, and C targets.

This provides a good fit to all of the data for lower Z beams in hydrogen, helium, and carbon targets. In Fig. 10, we show the value of the effective overlap parameter b in Eq. (8) as a function of A_B and A_t that is required to give the same σ as Eq. (10). This dependence of b on A_B and A_t has many similarities to the predictions of the soft sphere model of Karol.[14] In Fig. 10, we also show the value of b in Eq. (8) required to fit the high Z beam data of Binns *et al.*[7] Equation (10) provides a good fit to all of the data for carbon targets, but for hydrogen targets, the value of b' is required to increase in order to fit the high Z beam data, indicating a rapid increase in the overlap parameter or conversely a greater transparency in the nuclear reaction cross section.

ACKNOWLEDGMENTS

We owe a special thanks to many people at Lawrence Berkeley Laboratory for making arrangements and for assisting us in the runs at the Bevalac. In particular we wish to thank Fred Lothrop and Hank Crawford. We also thank our many colleagues who have offered suggestions during the course of this program and in the data analysis. This program has been supported by NASA Grants NGR 30-002-052 and NAG 8-468.

[1]W. R. Webber, Astrophys. J., **252**, 386 (1982).
[2]W. R. Webber and D. A. Brautigam, Astrophys. J. **260**, 894 (1982).
[3]P. Ferrando, W. R. Webber, P. Goret, J. C. Kish, D. Schrier, A. Soutoul, and A. Testard, Phys. Rev. C **37**, 1490 (1988).
[4]D. E. Greiner, P. J. Lindstrom, H. H. Heckman, B. Cork, and F. S. Bieser, Phys. Rev. Lett. **35**, 152 (1975).
[5]H. H. Heckman, D. E. Greiner, P. J. Lindstron, and F. S. Bieser, Phys. Rev. Lett. **28**, 926 (1972).
[6]G. D. Westfall, L. W. Wilson, P. J. Lindstrom, H. J. Crawford, D. E. Grenier, and H. H. Heckman, Phys. Rev. C **19**, 1309 (1979).
[7]W. R. Binns, T. L. Garrard, M. H. Israel, M. P. Kertzmann, J. Klarmann, E. C. Stone, and C. J. Waddington, Phys. Rev. C **36**, 1870 (1987).
[8]P. U. Renberg, D. F. Measday, M. Pepin, P. Schwaller, B. Favier, and C. Richard Serie, Nucl. Phys. **A183**, 81 (1972).
[9]B. M. Bobchenko *et al.*, Yad. Fiz. **30**, 1553 (1979) [Sov. J. Nucl. Phys. **30**, 805 (1979)].
[10]J. R. Letaw, R. Silberberg, and C. H. Tsao, Astrophys. J. Suppl. **51**, 271 (1983).
[11]C. Brechtmann and W. Heinrich, Proc. 20th ICRC **2**, 137 (1987).
[12]W. R. Webber, J. C. Kish, and D. A. Schrier, Phys. Rev. C **41**, 547 (1990), this issue.
[13]P. J. Lindstrom, D. E. Greiner, H. H. Heckmann, B. Cork, and F. S. Bieser, Lawrence Berkeley Laboratory Report No. 3650, 1975.
[14]P. J. Karol, Phys. Rev. C **11**, 1203 (1975).